Saturable time-varying mirror based on an epsilon-near-zero material

Romain Tirole,[1,*] Emanuele Galiffi,[1,2] Jakub Dranczewski,[1] Taran Attavar,[1] Benjamin Tilmann,[3] Yao-Ting Wang,[2] Paloma A. Huidobro,[4] Andrea Alú,[2,5] John B. Pendry,[1] Stefan A. Maier,[1,3] Stefano Vezzoli,[1] and Riccardo Sapienza[1,†]

[1] *The Blackett Laboratory, Department of Physics, Imperial College London, London SW7 2BW, United Kingdom*
[2] *Photonics Initiative, Advanced Science Research Center, City University of New York, 85 St. Nicholas Terrace, 10031, New York, NY, USA*
[3] *Chair in Hybrid Nanosystems, Nanoinstitut München, Ludwig-Maximilians-Universität München, 80539 München, Germany*
[4] *Instituto de Telecomunicações, Instituto Superior Tecnico-University of Lisbon, Avenida Rovisco Pais 1, Lisboa, 1049-001 Portugal*
[5] *Physics Program, Graduate Center, City University of New York, New York, NY 10016, USA*

(Dated: October 26, 2022)

We report a switchable time-varying mirror, composed of an Indium Tin Oxide - Gold bilayer, displaying a ten-fold modulation of reflectivity ($\Delta R \approx 0.6$), which saturates for a driving pump intensity $I_{\text{pump}} \approx 100$ GW/cm^2. Upon interacting with the saturated time-varying mirror, the frequency content of a reflected pulse is extended up to 31 THz, well beyond the pump spectral content (2.8 THz). We interpret the spectral broadening as a progressive shortening of the mirror rise time from 110 fs to sub 30 fs with increasing pump power, which is confirmed by four-wave mixing experiments and partially captured by a linear time-varying model of the mirror. A temporal response unbounded by the pump bandwidth enables applications for spectral manipulation from time-varying systems with impact for communication networks, optical switching and computing.

I. INTRODUCTION

Fundamental wave phenomena such as refraction and reflection rely on altering the wavevector of a wave by spatially modulating the permittivity, e.g. in a metamaterial. Conversely, a structured permittivity in the time domain manipulates the wave frequency. Time-varying systems are a platform for a wealth of exotic physics [1], including nonreciprocity [2–4], amplification [5, 6] and topology [7–10], as well as quantum-relativistic effects [11, 12], promising applications including photonic refrigeration [13] and temporal aiming [14]. However, bridging the gap between theory and experiment in time-varying systems has proven especially challenging at optical frequencies and ultrafast time-scales. Until recently, optical experiments have been mostly confined to silicon waveguides [15], micro-ring resonators [16] or slow-light photonic crystals [17], but at the cost of a narrow bandwidth and a slow temporal response.

In contrast, nonlinear optical interactions in epsilon-near-zero (ENZ) materials, such as transparent conducting oxides (TCOs) [18–22], as Indium-Tin-Oxide (ITO), can induce modulations of the permittivity on sub-picosecond time scales [23] with order-of-unity refractive index changes [19].

Time-varying physics have been observed in TCOs, with effects such as time-refraction [24–27] and time-reversal [28] of pulses, as well as in hybrid metal-dielectric metasurfaces with strong-ultrafast switching [29, 30], frequency shifting [23, 26, 31–33], polarisation switching [34] and high-harmonic generation [35]. Frequency shifts as large as 11 THz were achieved in a bulk 610 nm thick film of ITO [24]. However, the translation to thinner films, below 100 nm, has proven challenging due to the lack of interaction volume and propagation length within the active medium, with shifts limited to 1-2 THz [23, 25, 33]. Time-varying effects have been boosted by exploiting optical resonances both in all-dielectric [36–39] and hybrid plasmonic-ENZ metasurfaces [23, 32, 40], albeit limited by damage thresholds lower than in bulk ITO. Large modulation amplitudes, with no spectral dynamics study, have been achieved by exploiting the Berreman resonance in GaN[41].

Here, we exploit the Berreman absorption resonance of a layered ITO-gold bilayer as a switchable time-varying mirror. We demonstrate experimentally and model theoretically an ultrafast modulation of its reflection coefficient, which leads to an absolute reflectivity change $\Delta R \approx 0.6$ ($\Delta R/R \approx 1000\%$), which saturates for a pump intensity $I_{\text{pump}} \approx 100$ GW/cm^2. For optical pumping beyond saturation we observe the generation of new frequencies in the reflected probe spectrum which extend to a 31 THz range. We interpret this as a shortening of the response time of the time-varying mirror, which we confirm with a four-wave-mixing experiment.

* Corresponding author: romain.tirole16@imperial.ac.uk
† r.sapienza@imperial.ac.uk

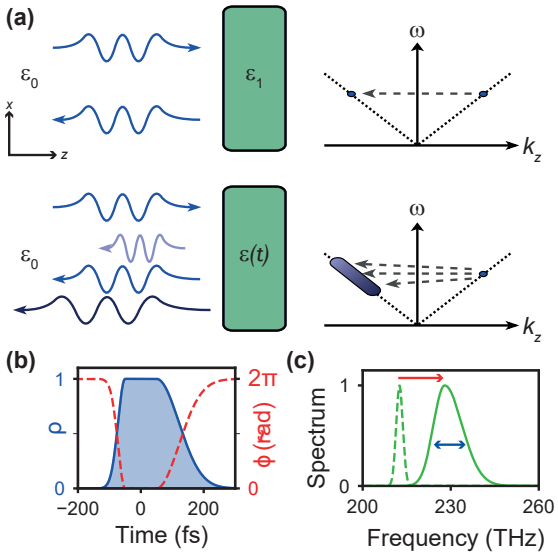

FIG. 1. **(a)** Concept of a purely time-varying mirror: reflection is a transition from k_z to $-k_z$ for the static mirror (top right), while the frequency distribution broadens for the time-varying mirror (bottom right). **(b)** Diagram of the temporal evolution of the complex reflection coefficient in amplitude (blue) and phase (red). **(c)** Spectral evolution of a pulse reflected by the time-varying mirror: an incoming pulse (dashed green) is shifted (red arrow) and broadened (blue arrow) in frequency (continuous green) due the respective changes in phase and amplitude of the reflection coefficient.

II. THE TIME-VARYING MIRROR

In a subwavelength and ultrafast time-varying mirror, as depicted in Fig.1(a), an incident light pulse is reflected with a time-varying complex reflection coefficient $r(t) = \rho(t)\exp[i\phi(t)]$. As illustrated qualitatively in Fig.1(b-c), a quick decrease of the Fresnel coefficient amplitude $\rho(t)$ leads to a temporal narrowing and consequently to a spectral broadening of the reflected pulse, while a change of phase $\phi(t)$ leads to a spectral shift.

An ideal time-varying mirror should be able to provide a large change in its complex reflection coefficient, close to unity in amplitude, so that it can be completely switched on and off, and with a phase shift of order π radians, over time-scales of the order of the optical period (∼fs), in order to give rise to significant spectral modulation.

We study a subwavelength time-varying mirror made of a 40 nm thin film of ITO with ENZ frequency $f_{\mathrm{ENZ}} \approx 227$ THz, deposited on glass and covered by a 100 nm gold layer as depicted in Fig.2(a). An optical pump pulse is used to modulate the mirror reflectivity, whereas a probe beam is used to measure the induced changes. The structure is much thinner than the effective wavelength in the layer (~ 6.6 µm at f_{ENZ}). Thin films of ENZ materials exhibit plasmonic ENZ modes (black line in Fig.2(b)) beyond the light cone, as well as a Berreman mode above the light line (red-marked reflectance dip (see Supplemental Material (SM) for details [42]) [43]. The deeply-subwavelength thickness of the system allows efficient coupling to the resonant guided Berreman mode from free space, while the reflective gold layer increases the confinement of the mode into the ITO film, enabling strong nonlinear interactions[35]. As shown in Fig.2(c), experimental evidence of the efficient coupling to the Berreman mode is manifested in the strong reflectivity dip measured at an angle of 65° close to the Brewster angle, for frequencies just below f_{ENZ} (230 THz, 1300 nm), which we choose as the working frequency for both the pump and the probe beam in our time-varying experiment. This compares very well to the theoretical prediction shown in Fig.2(d). The broad angular dependence of the Berreman mode ($\approx 60°$ to 70°) allows for the resonant coupling of both pump and probe beams.

The reflectivity of the ITO/Au mirror can be efficiently modulated by an ultrafast laser pulse, because of the consequent reduction in the plasma frequency following a change of the photocarrier dynamics in the ITO layer [30, 44]. The plasma frequency f_p shift is assumed to be proportional to the pump intensity [33] in our model (see SM [42]). This reduction in f_p is due to pump-induced intraband electronic transitions to states with higher effective mass [44]. From this model, we predict the evolution of the reflection modulation with increasing pump intensity, shown in Fig.2(e): the reflectivity is expected to reach a plateau for a driving intensity ∼100 GW/cm^2, which is confirmed by the data (blue crosses). Pump and probe beams are degenerate at the Berreman frequency (230 THz), the pump is incident at 75° and the probe at 65°. The mirror total reflectivity changes from $R = 0.07$ (without pump) and converges to $R = 0.66$ at intensities above saturation ($I_{\mathrm{sat}} \approx 100$ GW/cm^2), corresponding to an observed modulation of $\Delta R/R$ ∼1000%, as plotted in Fig.3(a). When the reflectivity of the glass substrate $R_s = 0.04$, which is not modulated, is subtracted, the observe reflectivity change is as high as 2200%.

This saturation of the reflection modulation can be explained by the redshift of the Berreman mode with f_p, illustrated in Fig.2(f): once the Berreman reflectivity dip is shifted far enough from its original frequency, the reflectivity reaches its highest value (Fig.2(g)). The role of the Berreman resonance is to increase the contrast of the maximum achievable modulation, as illustrated in Fig.2(e-g), and to enhance the pump intensity in the ITO layer. We point out that nonlinear effects in both the silica substrate and the gold layer can be neglected, since the Kerr coefficient of silica is 4 orders of magnitude smaller than that of ITO, whereas for gold, only a small portion

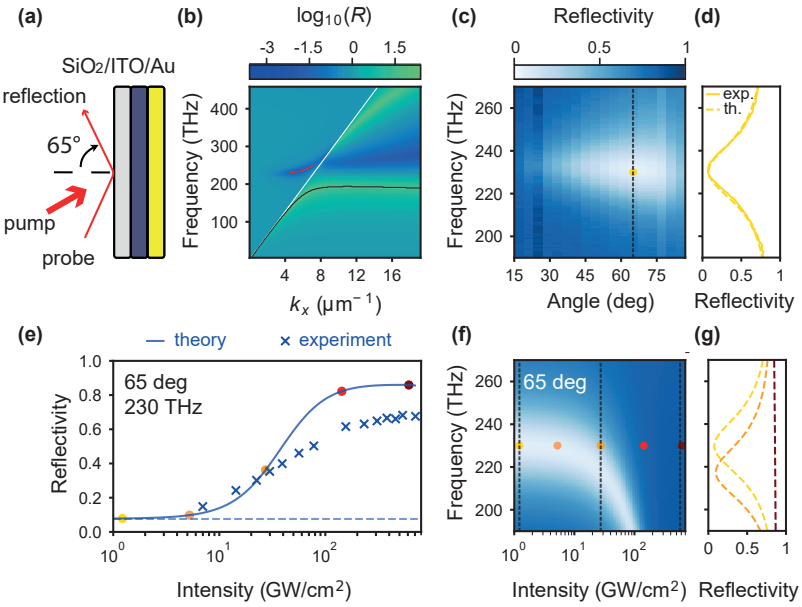

FIG. 2. **(a)** Sketch of a pump-probe experiment. **(b)** Dispersion diagram of the Berreman mode (red line), situated above the light line (white line), and of the plasmonic ENZ mode (black line). **(c)** Experimental reflectivity of the sample, versus angle and frequency. The black dashed line indicates the angle of 65° at which the reflectivity in panel **(d)** is shown. **(d)** Experimental (continuous blue) and numerically obtained (dotted blue) reflectivity of the sample at an incidence angle of 65°. **(e)** Experimental and expected reflectivity at 230 THz as a function of pump intensity. The coloured dots identify the reflectivity for a few powers as in (f). **(f)** Simulated shift of the Berreman resonance spectrum as a function of pump intensity for an illumination angle of 65°. The dashed grey lines indicate the intensities at which the spectra in panel (g) are shown. **(g)** Simulated reflectivity spectra of the sample under incident intensities of 1, 27 and 613 GW/cm^2.

of the field (3.7%) penetrates the gold layer, and its Kerr coefficient is still smaller than in ITO. The combination of these features, together with the large damage threshold of ITO, makes the Berreman mode a convenient platform to explore time modulations in a strongly non-perturbative pumping regime, i.e. well above the saturation of the reflectivity modulation.

III. SPECTRAL DYNAMICS OF THE SATURATED MEDIUM

So far, we have discussed the maximum achievable modulation and the mechanism leading to the saturation of reflectivity. We now turn to discuss the time dynamics of the mirror. The reflectivity changes are driven by pump pulse of finite duration (220 fs and 2.8 THZ, or 16 nm, bandwidth) and probe by an identical pulse. The evolution of the probe reflectivity with the pump/probe delay is illustrated in Fig.3(a) for different pump powers. The reflectivity rise time is given by the convolution between the pump pulse and the faster material response of ITO (below 50 fs [23], set at 30 fs in our model). The reflectivity decay time, on the other hand, is dominated by the slower relaxation dynamics of ITO ($\approx$ 360 fs [19]). Beyond $I_{\rm sat}$, after a sharp rise, the reflectivity reaches a plateau and features a longer decay time (yellow and red lines in Fig.3(a)). Our numerical simulations reproduce the temporal dynamics with good accuracy at low pump intensity (dashed blue line in Fig.3(a)), but overshoot in amplitude and fail to capture the longer decay time and the flattening of the response at high pump intensities.

In order to characterise the time-varying effects of the mirror, we focus on the spectral features of the probe signal undergoing modulation. Fig.3 shows the measured (b) and simulated (d) evolution of the probe spectrum at various delays, for a pump power of $I_{\rm pump}$ = 22 GW/cm^2, well below saturation. A successive thinning and broadening in the spectrum around zero delay is observable in Fig.3(b), associated with the amplitude change of the reflection coefficient. Overall the probe spectral content is largely unchanged, as shown in Fig.3(f) where the modulated (pink line) and unmodulated (light blue line) spectra are almost superposed.

These below-saturation dynamics, including the fine features around zero-delay, are well reproduced by the linear time-varying model shown in Fig.3(d). Since the modulation is significantly faster during the rise time, the time evolution of

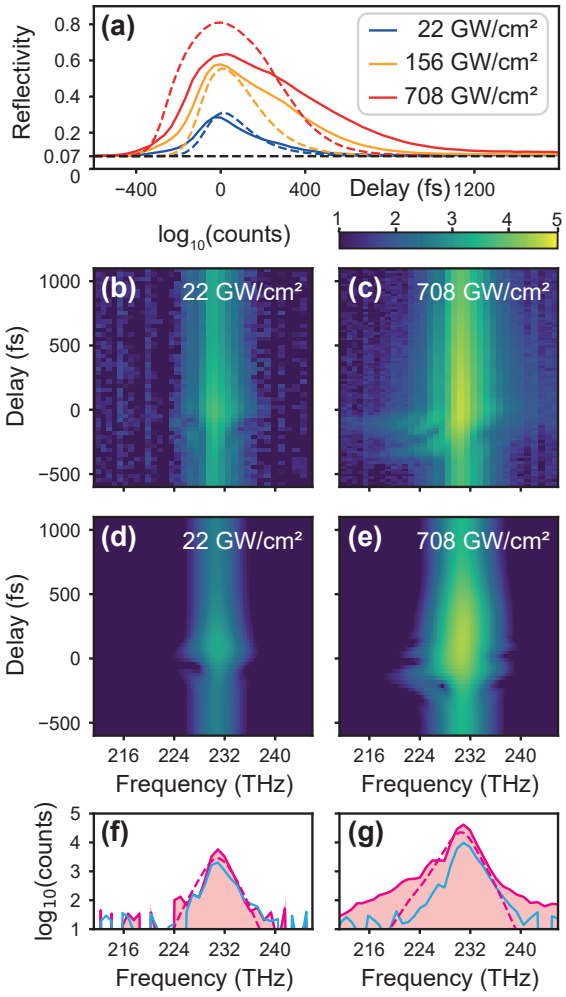

FIG. 3. **(a)** Experimental (continuous line) and numerically simulated (dashed line) evolution of the probe reflection as a function of the pump/probe delay for three pump intensities. **(b-e)** Comparison of the reflection as a function of delay and frequency, on a log scale, at low intensity (22 GW/cm^2, (b) experiment, (d) theory) and at high intensity (708 GW/cm^2, (c) experiment, (e) theory). **(f,g)** Cross-section of the experimental reflection signal shown in (b-c), at a delay of −90 fs (pink line) as well as -500 fs delay (light blue line) where no modulation happens. Numerically simulated modulated spectra from (d,e) are shown in dashed pink.

the spectrum is not symmetric and neither is the amount of blue and red shift at different delays.

In Fig.3(c) we present the spectral map for the maximum pump intensity achievable in our setup, $I_{\text{pump}} = 708$ GW/cm^2, well beyond I_{sat}. New frequencies are generated beyond the bandwidth of the unmodulated spectrum. This is qualitatively similar to what is predicted by our model and plotted in Fig.3(e) and in Fig.3(g) where new frequencies are observed (pink line) well beyond the frequency content of the unmodulated case (light blue line). The broadening and shift of the central part of the spectrum is well captured by the time-varying model (pink dashed line), however tails are much larger than predicted. Fringes extended from 214 to 245 THz appear in the map of Fig.3(c), well beyond the bandwidth (2.8 THz) of the modulating pump pulse. The spectral broadening is about 31 THz at an intensity of 10^{-3} of the modulated pulse, 10x higher than the noise level and it is largest at slightly negative delay (−90 fs), on the rise time of the mirror reflectivity, when the temporal gradient of reflectivity is at its maximum. Moreover, the spectrum becomes visibly asymmetric, with a clear inclination towards the red, due to change of phase in time. The full width at half maximum (FWHM) on the spectrum, however, is only marginally affected with an increase of 0.2 THz and a maximum recorded shift of 0.3 THz. The low amplitude of the newly generated frequencies can be explained by the probe pulse, which is longer than the medium rise time, and therefore only partially modulated. Our simple time varying model predicts a shortening of rise time when saturating the mirror reflection coefficient, going from the original 110 fs (pump limited) to about 60 fs. However, the mismatch between the data and the model in the tails of Fig.3(g) suggests that the rise time could be much shorter, pointing to richer material dynamics emerging under saturation conditions. We stress that our data shows the limits of the commonly accepted and used modelling of photo-induced shift of plasmonic resonances.

IV. SIGNATURE OF TEMPORAL DYNAMICS IN FOUR-WAVE-MIXING

The acceleration of the response time with increasing pump intensity can be measured more precisely with a four-wave-mixing (FWM) experiment. FWM is only generated when pump and probe beams interact inside the ITO layer, during the switching on of the time-varying mirror. .

The measured FWM signal as a function of pump/probe delay is shown in Fig.4(a) (solid red line). As expected, FWM generation mainly occurs during the rise time of the reflection (blue line in Fig.4(a)), as also confirmed by numerical simulation (dashed red line, see SM [42]). A high FWM efficiency of 7.5%, defined as the ratio of FWM power to the input probe power, is observed for a pump intensity of 612 GW/cm^2 (see Fig. S4 in SM [42]). In Fig.4(b) we plot the FWM spectrum as a function of the pump intensity for a delay of about −150 fs, where the FWM signal is maximum. The spectrum starts from a nearly Gaussian shape centered at 231 THz and with a width of 3.2 THz at a pump intensity of 15 GW/cm^2, very close to the original probe spectrum (2.8 THz).

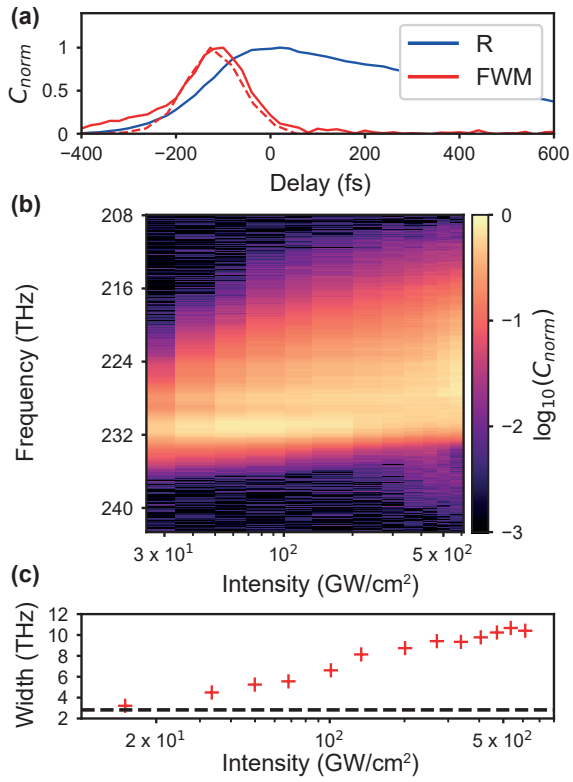

FIG. 4. **(a)** Measured evolution with pump/probe delay of the FWM signal (continuous red line) versus reflection (blue line). Simulated FWM signal is shown by the red dashed line. **(b)** Measured evolution of the FWM spectrum as a function of pump intensity: the spectrum gets broader with pump power, reaching a maximum bandwidth of 10.7 THz (61.5 nm) and a redshift of 3.8 THz (22 nm) for a pump intensity of 535 GW/cm^2. **(c)** Measured broadening of the FWM signal as a function of pump intensity (red crosses), compared with the spectral width of the original input probe spectrum (dashed black line).

This spectrum evolves towards a broad distribution with a FWHM of 10.7 THz (61.5 nm) for pump powers of ∼600 GW/cm^2, and which is also red-shifted by about 3.8 THz.

The width of the FWM signal shown in Fig.4(b) is plotted in Fig.4(c). The spectral width is taken here at the FWHM, as the time modulation affects the whole FWM spectrum, unlike the probe reflection. Therefore, from this 3.8x increase in bandwidth, we can estimate that the rise time of the time-varying mirror shortens to ∼ 30 fs. The FWM spectral broadening slows down around ∼400 GW/cm^2, as the medium reaches its intrinsic rise time. The value of 30 fs estimated from FWM data is likely an overestimate, as FWM is a complex process and other effects come into play in determining its bandwidth.

V. CONCLUSION

In conclusion, we have presented a saturable time-varying mirror based on the Berreman resonance of an ITO-Au thin film, exhibiting a record modulation of over 1000% in reflectivity. When pumping above the saturation level of the mirror response, new frequencies are generated, as far as 5 bandwidths away from the original carrier frequency, as confirmed by FWM measurements. We interpret the spectral broadening as a progressive acceleration of the mirror response time, which can be controlled by simply adjusting the pump pulse intensity, and not its duration, when in the non-perturbative regime [26, 35]. This demonstration of beyond-bandwidth rise time, through spectral rather than transient characterisation, unlocks further mechanisms for experiments in the field of time-varying systems. Although the Berreman resonance of the ITO/Au bilayer allows access to the saturation regime for a moderate pump intensity of 100 GW/cm^2, our results are very general and similar dynamics could emerge in other resonant architectures, once the strong saturation of their response is reached. The extent of the generated frequencies in both the reflection and the FWM spectra, pointing at a shortening of the rise time beyond the adiabatic limit, calls for a further development of the theory of photocarrier dynamics in ITO and ENZ media in the non-adiabatic regime and for a deeper understanding of the physical origin of saturation.

The results described here show the potential for efficient spectral manipulation of light, unlocking applications such as pulse shaping and temporal holograms. They represent a firm step towards the experimental realisation of fundamental concepts like time crystals, time diffraction and spatiotemporal metasurfaces.

ACKNOWLEDGMENTS

R.S., J.P., and S.V. acknowledge funding from the Engineering and Physical Sciences Research Council (EP/V048880), J.P. from the Gordon and Betty More Foundation, E.G. from the EPSRC (EP/T51780X/1) and the Simons Society of Fellows (855344,EG), A.A. the Department of Defense, the Simons Foundation, and the AFOSR MURI program, P.A.H. from FCT (UIDB/50008/2020 and CEECIND/02947/2020).

DATA AVAILABILITY

Data and codes are available upon request.

[1] E. Galiffi, R. Tirole, S. Yin, H. Li, S. Vezzoli, P. A. Huidobro, M. G. Silveirinha, R. Sapienza, A. Alù, and J. Pendry, Photonics of time-varying media, Adv. Photonics **4**, 014002 (2022).

[2] D. L. Sounas and A. Alú, Non-reciprocal photonics based on time modulation, Nat. Photonics **11**, 774 (2017).

[3] T. T. Koutserimpas and R. Fleury, Nonreciprocal gain in non-hermitian time-floquet systems, Phys. Rev. Lett. **120**, 087401 (2018).

[4] P. A. Huidobro, E. Galiffi, S. Guenneau, R. V. Craster, and J. B. Pendry, Fresnel drag in space-time-modulated metamaterials, PNAS **116**, 24943 (2019).

[5] E. Galiffi, P. Huidobro, and J. B. Pendry, Broadband nonreciprocal amplification in luminal metamaterials, Phys. Rev. Lett. **123**, 206101 (2019).

[6] M. C. Braidotti, A. Vinante, G. Gasbarri, D. Faccio, and H. Ulbricht, Zel'dovich amplification in a superconducting circuit, Phys. Rev. Lett. **125**, 140801 (2020).

[7] Q. Lin, M. Xiao, L. Yuan, and S. Fan, Photonic weyl point in a two-dimensional resonator lattice with a synthetic frequency dimension, Nat. Commun. **7**, 1 (2016).

[8] E. Lustig, Y. Sharabi, and M. Segev, Topological aspects of photonic time crystals, Optica **5**, 1390 (2018).

[9] L. He, Z. Addison, J. Jin, E. J. Mele, S. G. Johnson, and B. Zhen, Floquet chern insulators of light, Nat. Commun. **10**, 1 (2019).

[10] A. Darabi, X. Ni, M. Leamy, and A. Alù, Reconfigurable floquet elastodynamic topological insulator based on synthetic angular momentum bias, Sci. Adv. **6**, eaba8656 (2020).

[11] P. D. Nation, J. R. Johansson, M. P. Blencowe, and F. Nori, Colloquium: Stimulating uncertainty: Amplifying the quantum vacuum with superconducting circuits, Rev. Mod. Phys. **84**, 1 (2012).

[12] M. C. Braidotti, D. Faccio, and E. M. Wright, Penrose superradiance in nonlinear optics, Phys. Rev. Lett. **125**, 193902 (2020).

[13] S. Buddhiraju, W. Li, and S. Fan, Photonic refrigeration from time-modulated thermal emission, Phys. Rev. Lett. **124**, 077402 (2020).

[14] V. Pacheco-Peña and N. Engheta, Temporal aiming, Light. Sci. Appl. **9**, 1 (2020).

[15] H. Lira, Z. Yu, S. Fan, and M. Lipson, Electrically driven nonreciprocity induced by interband photonic transition on a silicon chip, Phys. Rev. Lett. **109**, 033901 (2012).

[16] S. F. Preble, Q. Xu, and M. Lipson, Changing the colour of light in a silicon resonator, Nat. Photonics **1**, 293 (2007).

[17] T. Kampfrath, D. M. Beggs, T. P. White, A. Melloni, T. F. Krauss, and L. Kuipers, Ultrafast adiabatic manipulation of slow light in a photonic crystal, Phys. Rev. A **81**, 043837 (2010).

[18] N. Kinsey, C. DeVault, A. Boltasseva, and V. M. Shalaev, Near-zero-index materials for photonics, Nat. Rev. Mater. **4**, 742 (2019).

[19] M. Z. Alam, I. De Leon, and R. W. Boyd, Large optical nonlinearity of indium tin oxide in its epsilon-near-zero region, Science **352**, 795 (2016).

[20] L. Caspani, R. P. M. Kaipurath, M. Clerici, M. Ferrera, T. Roger, J. Kim, N. Kinsey, M. Pietrzyk, A. Di Falco, V. M. Shalaev, A. Boltasseva, and D. Faccio, Enhanced nonlinear refractive index in ϵ-near-zero materials, Phys. Rev. Lett. **116**, 233901 (2016).

[21] T. S. Luk, D. de Ceglia, S. Liu, G. A. Keeler, R. P. Prasankumar, M. A. Vincenti, M. Scalora, M. B. Sinclair, and S. Campione, Enhanced third harmonic generation from the epsilon-near-zero modes of ultrathin films, App. Phys. Lett. **106**, 151103 (2015).

[22] E. G. Carnemolla, L. Caspani, C. DeVault, M. Clerici, S. Vezzoli, V. Bruno, V. M. Shalaev, D. Faccio, A. Boltasseva, and M. Ferrera, Degenerate optical nonlinear enhancement in epsilon-near-zero transparent conducting oxides, Opt. Mater. Express **8**, 3392 (2018).

[23] K. Pang, M. Z. Alam, Y. Zhou, C. Liu, O. Reshef, K. Manukyan, M. Voegtle, A. Pennathur, C. Tseng, and X. e. a. Su, Adiabatic frequency conversion using a time-varying epsilon-near-zero metasurface, Nano. Lett. **21**, 5907 (2021).

[24] Y. Zhou, M. Z. Alam, M. Karimi, J. Upham, O. Reshef, C. Liu, A. E. Willner, and R. W. Boyd, Broadband frequency translation through time refraction in an epsilon-near-zero material, Nat. Commun. **11**, 2180 (2020).

[25] C. Liu, M. Z. Alam, K. Pang, k. Manukyan, J. Hendrickson, E. Smith, Y. Zhou, O. Reshef, H. Song, and R. e. a. Zhang, Tunable doppler shift using a time-varying epsilon-near-zero thin film near 1550 nm, Opt. Lett. **46**, 3444 (2021).

[26] V. Bruno, S. Vezzoli, C. DeVault, E. Carnemolla, M. Ferrera, A. Boltasseva, V. M. Shalaev, D. Faccio, and M. Clerici, Broad frequency shift of parametric processes in epsilon-near-zero time-varying media, Appl. Sci. **10**, 1318 (2020).

[27] M. Ferrera and E. G. Carnemolla, Ultra-fast transient plasmonics using transparent conductive oxides, J. Opt. **20**, 024007 (2018).

[28] S. Vezzoli, V. Bruno, C. DeVault, T. Roger, V. M. Shalaev, A. Boltasseva, M. Ferrera, M. Clerici, A. Dubietis, and D. Faccio, Optical time reversal from time-dependent epsilon-near-zero media, Phys. Rev. Lett. **120**, 043902 (2018).

[29] J. Bohn, T. S. Luk, C. Tollerton, S. W. Hutchings, I. Brener, S. Horsley, W. L. Barnes, and E. Hendry, All-optical switching of an epsilon-near-zero plasmon resonance in indium tin oxide, Nat. Commun. **12**, 1017 (2021).

[30] M. Taghinejad, H. Taghinejad, Z. Xu, Y. Liu, S. P. Rodrigues, K. Lee, T. Lian, A. Adibi, and W. Cai, Hot-electron-assisted femtosecond all-optical modulation in plasmonics, Adv. Mater. **30**, 1704915 (2018).

[31] M. Z. Alam, S. A. Schulz, J. Upham, I. De Leon, and R. W. Boyd, Large optical nonlinearity of nanoantennas coupled to an epsilon-near-zero material, Nat. Photonics **12**, 79 (2018).

[32] C. Liu, M. Z. Alam, K. Pang, K. Manukyan, O. Reshef, Y. Zhou, S. Choudhary, J. Patrow, A. Pennathurs, H. Song, Z. Zhao, R. Zhang, F. Alishahi, A. Fallahpour, Y. Cao, A. Almaiman, J. M. Dawlaty, M. Tur, R. Z. Boyd, and A. E. Willner, Photon acceleration using a time-varying epsilon-near-zero metasurface, ACS Photonics **8**, 716 (2021).

[33] J. Bohn, T. S. Luk, S. Horsley, and E. Hendry, Spatiotemporal refraction of light in an epsilon-near-zero indium tin oxide layer: frequency shifting effects arising from interfaces, Optica **8**, 1532 (2021).

[34] M. Taghinejad, H. Taghinejad, Z. Xu, K.-T. Lee, S. P. Rodrigues, J. Yan, A. Adibi, T. Lian, and W. Cai, Ultrafast control of phase and polarization of light expedited by hot-electron transfer, Nano. Lett. **18**, 5544–5551 (2018).

[35] Y. Yang, J. Lu, A. Manjavacas, T. S. Luk, H. Liu, K. Kelley, J.-P. Maria, E. L. Runnerstrom, M. B. Sinclair, and S. e. a. Ghimire, High-harmonic generation from an epsilon-near-zero material, Nat. Phys. **15**, 1022 (2019).

[36] M. R. Shcherbakov, P. P. Vabishchevich, A. S. Shorokhov, K. E. Chong, D.-Y. Choi, I. Staude, A. E. Miroshnichenko, D. N. Neshev, A. A. Fedyanin, and Y. S. Kivshar, Ultrafast all-optical switching with magnetic resonances in nonlinear dielectric nanostructures, Nano. Lett. **15**, 6985 (2015).

[37] M. R. Shcherbakov, S. Liu, V. V. Zubyuk, A. Vaskin, P. P. Vabishchevich, G. Keeler, T. Pertsch, T. V. Dolgova, I. Staude, I. Brener, and A. A. Fedyanin, Ultrafast all-optical tuning of direct-gap semiconductor metasurfaces, Nat. Commun. **8**, 17 (2017).

[38] M. R. Shcherbakov, K. Werner, Z. Fan, N. Talisa, E. Chowdhury, and G. Shvets, Photon acceleration and tunable broadband harmonics generation in nonlinear time-dependent metasurfaces, Nat. Commun. **10**, 1345 (2019).

[39] N. Karl, P. P. Vabishchevich, M. R. Shcherbakov, S. Liu, M. B. Sinclair, G. Shvets, and I. Brener, Frequency conversion in a time-variant dielectric metasurface, Nano. Lett. **20**, 7052 (2020).

[40] V. Bruno, C. DeVault, S. Vezzoli, Z. Kudyshev, T. Huq, S. Mignuzzi, A. Jacassi, S. Saha, Y. D. Shah, S. A. Maier, D. R. S. Cumming, A. Boltasseva, M. Ferrera, M. Clerici, D. Faccio, R. Sapienza, and V. M. Shalaev, Negative refraction in time-varying strongly coupled plasmonic-antenna–epsilon-near-zero systems, Phys. Rev. Lett. **124**, 043902 (2020).

[41] A. D. Dunkelberger, D. C. Ratchford, A. B. Grafton, V. M. Breslin, E. S. Ryland, D. S. Katzer, K. P. Fears, R. J. Weiblen, I. Vurgaftman, A. J. Giles, C. T. Ellis, J. G. Tischler, J. D. Caldwell, and J. C. Owrutsky, Ultrafast active tuning of the berreman mode, ACS Photonics **7**, 279–287 (2019).

[42] See Supplemental Material at [URL will be inserted by publisher] for detailed experimental methods, further characterisation of the time-varying effects in the sample, theoretical modelling, four-wave-mixing efficiency and a study of self-induced effects.

[43] S. Vassant, J.-P. Hugonin, F. Marquier, and J.-J. Greffet, Berreman mode and epsilon near zero mode, Opt. Express **20**, 23971 (2012).

[44] H. Wang, K. Du, C. Jiang, Z. Yang, L. Ren, W. Zhang, S. J. Chua, and T. Mei, Extended drude model for intraband-transition-induced optical nonlinearity, Phys. Rev. Applied **11**, 064062 (2019).